

Theoretical study of the charge transfer and electron emission in the scattering of He^+ by an AlF_3 surface

A. Iglesias-García,¹ C. González,² and E. C. Goldberg^{1,3}

¹*Instituto de Física del Litoral (CONICET-UNL) Güemes 3450 (S3000GLN) Santa Fe, Argentina*

²*Departamento de Física Teórica de la Materia Condensada and Condensed Matter Physics Center (IFIMAC), Facultad de Ciencias, Universidad Autónoma de Madrid, 28049 Madrid, Spain*

³*Departamento de Ingeniería en Materiales - Facultad de Ingeniería Química, UNL (S3000GLN) Santa Fe, Argentina*

(Received 17 May 2017; published 21 August 2017)

Experimental results of electron emission from surfaces of aluminum fluoride impacted by keV noble gas ions (He^+ , Ne^+ , Ar^+) show a high-energy structure that increases in intensity with ion energy in the case of He^+ and Ar^+ and is nearly independent on the impact energy for Ne^+ ions. It is also observed that this high-energy secondary electron peak is less pronounced in the case of impact by Ar^+ . While ion-induced electron emission in metal surfaces is relatively well understood, in the case of wide band-gap insulators, such as metal fluorides, the nature of high-energy excitations is still an open question. In this work, we propose a mechanism of high-energy electron emission strongly linked to the ion neutralization process and the collision induced excitation of the electrons in the solid.

DOI: [10.1103/PhysRevB.96.075428](https://doi.org/10.1103/PhysRevB.96.075428)

I. INTRODUCTION

The AlF_3 is a good insulator, with a wide band-gap of 10.8 eV, and a good passivating agent due to its rather inert chemically behavior [1]; it readily decomposes upon irradiation with low- or mid-energy electrons [2–4], releasing molecular fluorine and leaving a deposit of metallic Al on the substrate, which makes AlF_3 an attractive inorganic resist for e-beam nanopatterning techniques [5,6]. All these characteristics turns AlF_3 a useful material for diverse applications such as solar cell technology [1], molecular biology [7], and fabrication of dilute magnetic semiconductors [8,9].

The behavior of these wide band-gap insulators under the ion bombardment is not only interesting from a technological point of view, because of the applications to astrophysics and nanotechnology, but also from a fundamental point of view. Electron emission is a primary effect occurring during the irradiation of a surface by low energy ions. The mechanisms of electron emission are divided, according to the energy source, into potential and kinetic emission [10,11]. While ion-induced electron emission in metal surfaces is relatively well understood, the situation is different with wide band-gap insulators, such as metal fluorides, where the nature of high-energy excitations is a matter of current debate.

In this work, we focus on the measurements of electron emission spectra from surfaces of aluminum fluoride impacted by keV noble gas ions (He^+ , Ne^+ , Ar^+), which show a high-energy structure, clearly differentiated from the low-energy electrons that result from the electron collision cascade in the solid, that increases in intensity with ion energy in the case of He^+ and Ar^+ ions and is nearly independent on the impact energy for Ne^+ ions [12]. These dependencies are different from the decreasing with impact energy behavior observed in the secondary electron spectra coming from a clean copper surface bombarded by He^+ and Ne^+ , where a potential emission due to the Auger neutralization mechanism occurs [13]. From this comparative analysis, it is possible to conclude that the emission of high-energy electrons, in the case of AlF_3 , is kinetic. The experimental results also show that the shape of

the spectra is independent of the type of ion, suggesting that it is dominated by the electronic states of the solid. In Ref. [12], the authors propose as a possibility to explain the high-energy secondary electron peak, a two-electron excitations in fluorine. A doubly excited F^- state would decay by auto-ionization to $\text{F } 2p^5$ emitting an energetic electron.

We explore, in the present paper, another possibility for high-energy electron emission linked to the ion neutralization process and the collision induced excitation of electrons in the solid. In particular, we study the scattering of positive He ions from a AlF_3 surface by using a time-dependent Anderson Hamiltonian for describing the interacting system. The ion neutralization and the electron distribution in the surface after the collision are calculated by using the nonequilibrium Keldysh Green function formalism [14,15]. We find that electrons are promoted from the $\text{F-}2p$ valence band to the conduction band and holes are created in the strongly localized $\text{F-}2s$ band due to the ion neutralization. In this way, we show that the decay of excited electrons to the long-lived holes in the deep and narrow $\text{F-}2s$ band, can be a source of high-energy emitted electrons.

II. THEORY

The AlF_3 crystalline solid corresponds to a rhombohedral structure R-3c [16] such as the one shown in Fig. 1(a). The distances between atoms are 2.542 Å for F-F and 1.797 Å for Al-F; being the F-Al-F angle of 90° and the Al-F-Al angle of 157.07° . To our knowledge, the composition and the crystallography of AlF_3 thin films are not known. Experimental results [17,18] indicate that the film grown at room temperature completely covers the substrate, presenting no long-range crystallographic order and good AlF_3 insulator properties. This film would be stoichiometric, but terminated with two F atoms per Al one. All these observations lead to the proposal for the hexagonal unit cell shown in Fig. 1(b) with lattice parameters $a = b = 5.37$ Å and $c = 13.5$ Å. This unit cell contains six Al and 18 F, which is a total of 24 atoms. In this form a slab was

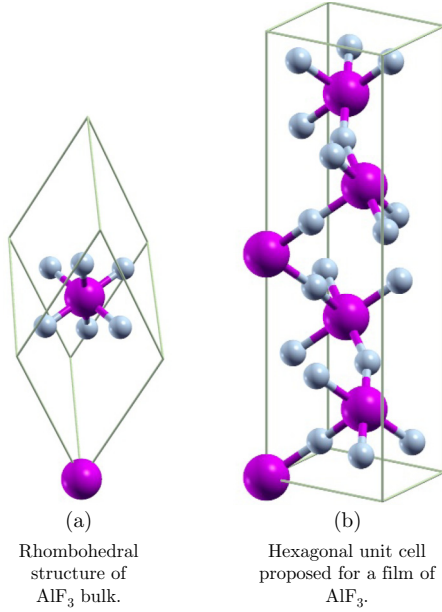


FIG. 1. α -AIF₃ crystal structure. The big spheres correspond to Al and the small ones to F atoms (the software Xcrsden [19] was used to draw these figures).

constructed by duplicating the unit cell in the c direction and by considering an empty space of 76.5 Å.

The FIREBALL code [20,21], based on the density functional theory (DFT) within the local density approximation (LDA), was used for calculating the density matrix of the α -AIF₃ (0001) film constructed in the form described above. The density matrix is given by the following expression:

$$\rho_{i\vec{R}_s; j\vec{R}_{s'}}(\varepsilon) = \sum_{\vec{k}} C_{i\vec{R}_s}^{\vec{k}*} C_{j\vec{R}_{s'}}^{\vec{k}} \delta(\varepsilon - \varepsilon_{\vec{k}}). \quad (1)$$

In Eq. (1), the index i denotes orbital and \vec{R}_s the atom position in the solid. The trace of this matrix is the local and partial density of states shown in Fig. 2.

The energy band gap is underestimated by the LDA approximation, therefore we have applied the scissors operator [22] to shift the calculated density of states and correct the band gap to its measured value (10 ± 0.2) eV [12]. The vacuum level (W_ϕ) is positioned at 12 eV with respect to the top of the valence band, that is a positive affinity for the AIF₃. We can observe from Fig. 2 a narrow valence band very localized around -20 eV, which has practically a pure F-2s character, and a predominantly F-2p band between -7 and 0 eV. The 3s and 3p Al states provide the main contribution to the conduction band.

The Auger neutralization process provides the main mechanism for potential emission. In this process an electron from the solid tunnels the surface barrier to neutralize the incoming projectile, and the excess energy is taken by another electron to escape from the solid [23]. In the case of insulators, where the work function is replaced by the sum of the band gap, electron affinity and hole-hole repulsion energy, a lower probability for electron emission is expected for ions of low velocities where potential emission is dominant for metals [24]. Then, even though the ionization potential of the He projectile,

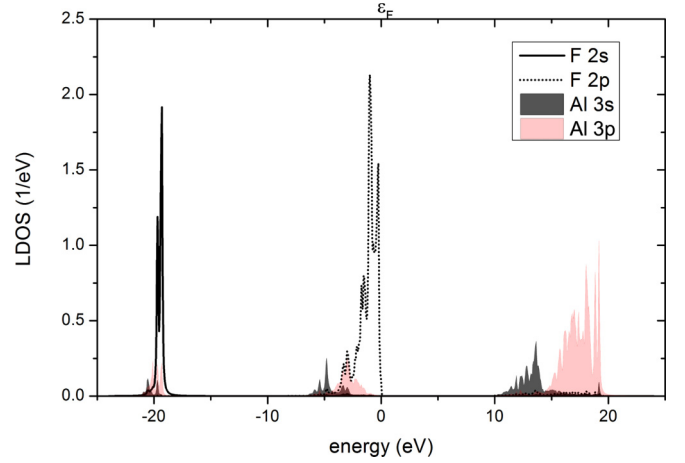


FIG. 2. Partial density of states of the α -AIF₃ (0001) surface. The contribution of F states to the s band is indicated by full lines and to the p band by dotted lines. Shaded regions correspond to the contribution of Al states. The zero energy is chosen at the top of the valence band.

-24.6 eV respect to the vacuum level, enables the Auger mechanism of neutralization, it is expected a low probability of occurrence in the range of incoming energies between 1 and 5 keV. On the other side, we are mainly interested in the kinetic emission of energetic electrons which arise from auto ionization of excitons, that are formed by electrons promoted to conduction band states close to the vacuum level and holes created in a strongly bound and localized band such as the F-2s one. Then, in this work we are only going to explore the He⁺ resonant neutralization, described by the following Anderson-like Hamiltonian within the spinless approximation, which results to be adequate in the case of neutralization of He⁺ to its ground state [24,25]:

$$\hat{H} = \sum_{\vec{k}} \varepsilon_{\vec{k}} \hat{c}_{\vec{k}}^\dagger \hat{c}_{\vec{k}} + \varepsilon_a \hat{c}_a^\dagger \hat{c}_a + \sum_{\vec{k}} [V_{ka} \hat{c}_{\vec{k}}^\dagger \hat{c}_a + \text{H.c.}]. \quad (2)$$

The first term in Eq. (2) has to do with the unperturbed solid target with one electron states $\psi(\vec{k})$ and energies $\varepsilon_{\vec{k}}$; the second one corresponds to the atom with ionization energy ε_a , and the third term describes the interaction between the solid and atomic states through the coupling integral V_{ka} . The fermionic operator $\hat{c}_{\vec{k}}^\dagger$ (\hat{c}_a) destroys an electron in a band(atom) state. In the ion-surface scattering process, both parameters, ε_a and V_{ka} , depends on time (t) because of the ion movement with finite velocity \vec{v} along a trajectory defined by $\vec{R} = \vec{R}(\vec{v}, t)$. The required Hamiltonian parameters are calculated by using the bond pair model [26], based on an adiabatic evolution along the ion trajectory and which has proved to provide a good description in many different atom-surface systems [18,24,25,27]. In this form, we obtain the distance to the surface dependence of the parameters, which then turns into a time dependence, when the ion movement with a finite velocity is considered. It is mainly based on the expansion of the solid states $\psi(\vec{k})$ in a atomic basis $\varphi_i(\vec{r} - \vec{R}_s)$ (i denotes orbital and \vec{R}_s the atom position) and a mean-field approximation to the electron-electron interactions, together with a symmetric orthogonalization procedure [28]. In this form, we have that the atom-band states coupling term V_{ka} is

calculated as a superposition of atom-atom couplings, $V_{i\bar{R}_s,a}^{\text{dim}}$, each one defined in the orthogonalized space of the dimer formed by the projectile atom and one atom of the solid:

$$V_{k,a} = \sum_{i,\bar{R}_s} C_{i\bar{R}_s}^k V_{i\bar{R}_s,a}^{\text{dim}}. \quad (3)$$

The expansion coefficients in Eq. (3) are the ones that define the density matrix, Eq. (1). The ionization energy is calculated as $\varepsilon_a = E_{\text{total}}^{\text{He}^0} - E_{\text{total}}^{\text{He}^+}$, without allowing charge transfer between atom and surface. The calculation includes the short range interactions electron-nucleus, nucleus-nucleus and electron-electron within a mean-field treatment, the overlap terms up to a second order in the overlap expansion [26], and also the interaction with the point charge field of the ionic surface (Madelung potential). For calculating this last interaction, we extract the values of the point charges from the DFT calculation of the surface.

A. Calculation of He^+ neutralization probability and energy distribution of emitted electrons

We are interested in calculating the neutral fraction

$$n_a(t) = \langle \hat{c}_a^\dagger \hat{c}_a \rangle_t \quad (4)$$

and the energy distribution of the emitted electrons

$$N(\varepsilon, t) = \sum_{\bar{k}} \langle \hat{c}_{\bar{k}}^\dagger \hat{c}_{\bar{k}} \rangle_t \delta(\varepsilon - \varepsilon_{\bar{k}}). \quad (5)$$

The procedure is based on the equations of motion of the mean values of both, the atomic occupation number $\hat{n}_a(t) = \hat{c}_a^\dagger(t) \hat{c}_a(t)$ and the band state occupation number $\hat{n}_{\bar{k}}(t) = \hat{c}_{\bar{k}}^\dagger(t) \hat{c}_{\bar{k}}(t)$; taking into account that they are in the Heisenberg representation, the following equations of motion result (atomic units are used):

$$\frac{d\langle \hat{n}_a(t) \rangle}{dt} = i \langle [\hat{H}(t), \hat{n}_a(t)] \rangle = 2 \text{Im} \sum_{\bar{k}} V_{ka}^*(t) \langle \hat{c}_a^\dagger \hat{c}_{\bar{k}} \rangle_t, \quad (6)$$

$$\frac{d\langle \hat{n}_{\bar{k}}(t) \rangle}{dt} = -2 \text{Im} V_{ka}^*(t) \langle \hat{c}_a^\dagger \hat{c}_{\bar{k}} \rangle_t. \quad (7)$$

From Eqs. (5) and (7), we can write

$$\frac{dN(\varepsilon, t)}{dt} = -2 \text{Im} \sum_{\bar{k}} V_{ka}^*(t) \langle \hat{c}_a^\dagger \hat{c}_{\bar{k}} \rangle_t \delta(\varepsilon - \varepsilon_{\bar{k}}). \quad (8)$$

The total number of electrons is a conserved quantity as it can be seen from Eqs. (6) and (8):

$$\frac{d\langle \hat{n}_a(t) \rangle}{dt} + \int_{-\infty}^{\infty} \frac{dN(\varepsilon, t)}{dt} d\varepsilon = 0. \quad (9)$$

Both quantities, $\langle \hat{n}_a(t) \rangle$ and $N(\varepsilon, t)$, require the calculation of the atom-band crossed term $\langle \hat{c}_a^\dagger \hat{c}_{\bar{k}} \rangle_t$, which is obtained from the following Green function [14,15]:

$$F_a(\hat{c}_{\bar{k}})(t, t') = i \langle [\hat{c}_a^\dagger(t'); \hat{c}_{\bar{k}}(t)] \rangle,$$

at equal times, $t = t'$, we have

$$F_a(\hat{c}_{\bar{k}})(t', t') = 2i \langle [\hat{c}_a^\dagger \hat{c}_{\bar{k}}] \rangle_{t=t'}. \quad (10)$$

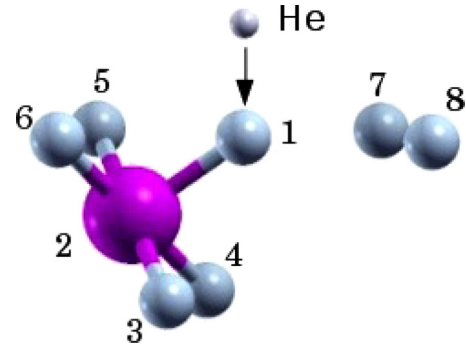


FIG. 3. The He^+ ion, indicated by the smallest sphere, is scattered by the F atom (1). The F and Al neighbors included in the ion-surface interaction process are shown. The biggest sphere corresponds to the Al atom.

The equation of motion of $F_a(\hat{c}_{\bar{k}})(t', t')$ leads to the result

$$F_a(\hat{c}_{\bar{k}})(t', t') = -i \int_{t_0}^t d\tau V_{ka}(\tau) [F_a(\tau, t) - (2\langle \hat{n}_{\bar{k}} \rangle_{t_0} - 1)G_a(\tau, t)] e^{i\varepsilon_{\bar{k}}(\tau-t)}. \quad (11)$$

In Eq. (11), $\langle \hat{n}_{\bar{k}} \rangle_{t_0}$ is the Fermi distribution. Finally, the calculation of the average value $\langle \hat{c}_a^\dagger \hat{c}_{\bar{k}} \rangle$ requires the knowledge of the Keldysh Green Functions projected on the atom state:

$$G_a(\tau, t) = i \Theta(t - \tau) \langle [\hat{c}_a^\dagger(t); \hat{c}_a(\tau)] \rangle,$$

$$F_a(\tau, t) = i \langle [\hat{c}_a^\dagger(t); \hat{c}_a(\tau)] \rangle, \quad (12)$$

which in turn are calculated from their equations of motion [25].

B. Calculation of the Hamiltonian terms

The AlF_3 surface and the scattering geometry we are going to consider are shown in Fig. 3. By taking into account the interaction of the projectile not only with the F atoms at the surface but also with the Al atom beneath, the ion neutralization and the electron-hole pair excitation are both well contemplated. The electrons come mainly from the F-like bands but the empty bands to receive the promoted electrons are provided by the aluminum.

The atom-atom coupling integrals of Eq. (3) are calculated by using the atomic basis set for F and Al given by Huzinaga [29,30]. In Fig. 4, we can observe in a comparative way the He-F and He-Al coupling terms as a function of the ion distance to the surface, z . At distances for which the interaction between atoms becomes effective, the coupling of the He-1s state with the s and p -states of the nearest F atom [Fig. 4(a)] is practically two orders of magnitude larger than the coupling with the other F atoms [Fig. 4(b)]. The coupling with the valence states of Al [Fig. 4(c)] show a more extended character and they are more significant than the coupling terms with the F atoms close to the scatter one.

The ion energy level variation with the distance to the surface is shown in Fig. 5 for the two possibilities: He^+ scattered by either the F or the Al atom in the scattering geometry of Fig. 3. The one electron energy level is obtained by considering the short range contributions in the total energy calculations

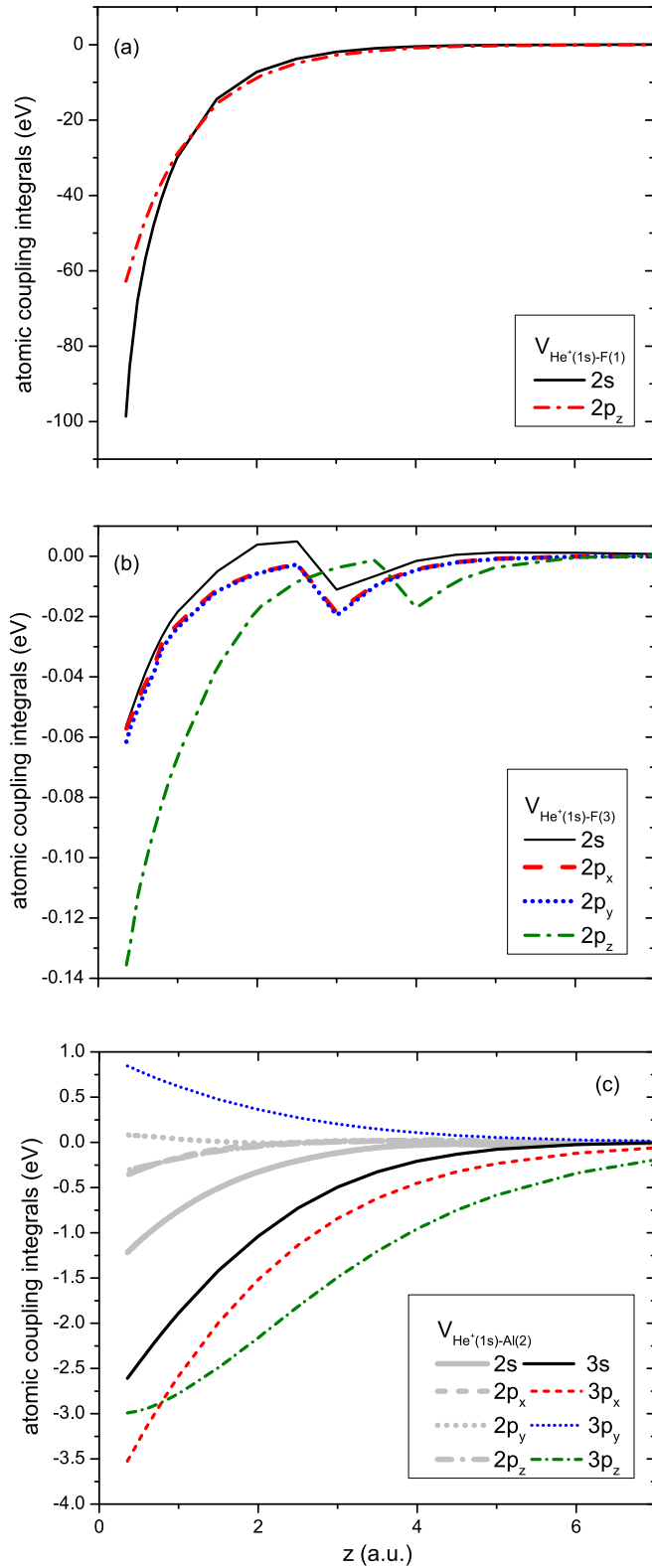


FIG. 4. (a) The coupling terms of He-1s state with the 2s and 2p states of the scatter F atom (atom 1 of Fig. 2). (b) The coupling terms of He-1s state with the 2s and 2p states of the F atom 3 of Fig. 3. (c) The coupling terms of He-1s state with the 2s, 2p, 3s, and 3p states of the Al, atom 2 of Fig. 3.

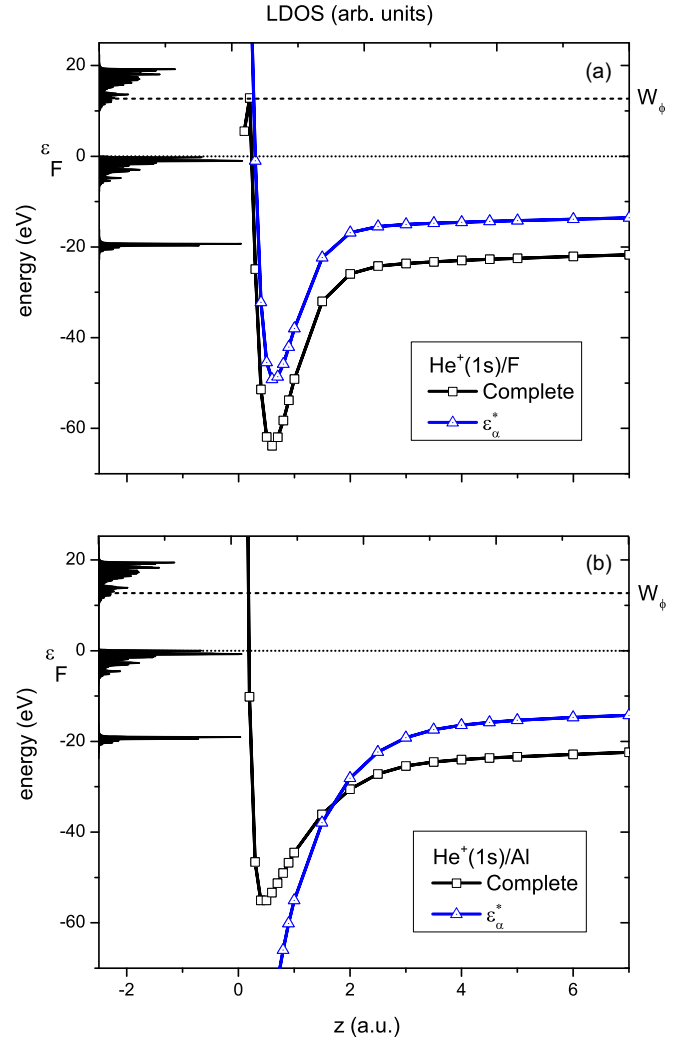


FIG. 5. (a) The He-1s energy level in front of a F atom of the AlF₃ surface (Fig. 3) by considering (square) and not (triangle) the Madelung potential. (b) The same as (a) in the case of helium in front of a Al atom. The energy levels are contrasted with the LDOS of the AlF₃ (0001) surface (shaded regions); the top of the valence band is chosen as the zero of energy and the vacuum level (W_ϕ) is indicated by the horizontal dash line.

($\varepsilon_{\text{He}^0}, \varepsilon_{\text{He}^+}$) and the Madelung potential, $V_{\text{MAD}}(z) = \sum_j q_{\text{He}^+} \cdot q_j / |\vec{z} - \vec{R}_j|$. In this form, we have that $\varepsilon_a(z)$ is given by

$$\begin{aligned} \varepsilon_a(z) &= E_{\text{total}}^{\text{He}^0}(z) - E_{\text{total}}^{\text{He}^+}(z) \\ &= \varepsilon_{\text{He}^0}(z) - (\varepsilon_{\text{He}^+}(z) + V_{\text{MAD}}(z)) \\ &= \varepsilon_a^*(z) - V_{\text{MAD}}(z). \end{aligned} \quad (13)$$

In Eq. (13), $\varepsilon_a^*(z)$ is the one electron energy without the Madelung contribution and it is also shown in Fig. 5 in order to appreciate the effect of the Madelung potential on the energy level shift. In both cases, the helium in front of either F or Al atom, we observe that the energy level including the Madelung potential seems to enable a resonant charge exchange process

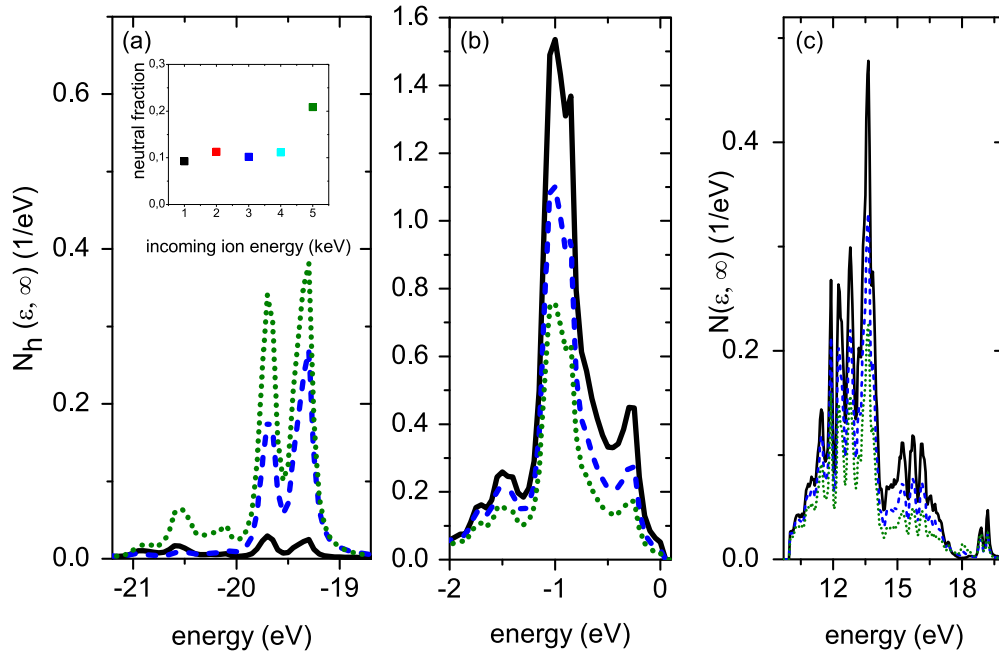


FIG. 6. (a) The energy distribution of holes $N_h(\epsilon, \infty)$ created in the F-2s band for incoming ion energies: 1 (solid line), 3 (dash line), and 5 (dot line) keV. (b) The same for holes created in the F-2p band. (c) Energy distribution of electrons excited to the conduction band $N(\epsilon, \infty)$. Equal y-axis scales are used in (a), (b) and (c). (Inset) Neutral fraction $n_a(t = \infty)$ as a function of the incoming ion energy.

only very close to the surface and also a promotion of the F-2s and F-2p electrons.

III. RESULTS AND DISCUSSION

As it is indicated in Fig. 3, the ion trajectory is assumed perpendicular respect to the surface and with a constant velocity, $z_{\text{in(out)}} = z_{\text{rtp}} + v_{\text{in(out)}}|t|$. The kinetic energy loss factor due to the elastic scattering of helium by a F atom, for a scattering angle equal to 180° , is 0.425. The considered ion kinetic energies are 1, 2, 3, 4, and 5 keV and the corresponding turning points, $z_{\text{rtp}} = 0.35, 0.2, 0.16, 0.12,$ and 0.1 a.u. were estimated from the interaction energy between He^+ and F⁻ atoms.

A. He^+ neutralization and energy distribution of holes and electrons created in the AlF_3 surface

The energy distribution of holes below the top of the valence band calculated as $N_h(\epsilon, \infty) = N(\epsilon, -\infty) - N(\epsilon, \infty)$ is shown in Figs. 6(a) and 6(b). The energy distribution of excited electrons, given by $N(\epsilon, \infty)$ for energy values corresponding to the initially empty conduction band states, is shown in Fig. 6(c). We can observe the behavior for the different incoming ion energies, the holes in the F-2s band increase with increasing kinetic energy [Fig. 6(a)], while the opposite behavior is observed for both, the case of holes in the F-2p valence band [Fig. 6(b)] and the case of electrons in the conduction band [Fig. 6(c)]. On the other hand, the neutral fraction shown in the inset of Fig. 6(a) has also a tendency to increase with energy, suggesting in this way that the helium neutralization occurs at the expense of F-2s band and the electrons of the F-2p band are excited due to the ion-surface collision process. That is clear from Fig. 7 where

we can see together the evolutions along the ion trajectory of the He-1s state occupation $\langle n_a \rangle$, the hole occupation of both F-2s and F-2p valence bands,

$$\int_{\epsilon \in [\text{F-2s band}]} N_h(\epsilon, z) d\epsilon \quad \text{and} \quad \int_{\epsilon \in [\text{F-2p band}]} N_h(\epsilon, z) d\epsilon;$$

and the electron occupation of the AlF_3 conduction band,

$$\int_{\epsilon \in \text{c.b.}} N(\epsilon, z) d\epsilon.$$

It is observed in Fig. 7 that for ion distances not very close to the surface, there is a clear correspondence between the holes created in the F-2s band and the electrons transferred to the helium state; and also between the holes created in the F-2p band and the electrons excited to the conduction band. At small distances from the surface, the mixing between the He state and the band states of AlF_3 is large enough as to make not possible a clear discrimination between them.

The neutral fraction is practically constant and around 10% for kinetic energies below 5 keV, being practically duplicated at 5 keV. By estimating the energy uncertainty of the atomic level due to the ion velocity [31], $\Delta E \approx v$ in atomic units, we found that at 5 keV the resonance between the projectile level and the F-2s band states begins to be favored at distances for which the interaction is effective ($z \approx 2-4$ a.u.).

The above results show that the proximity of the ion energy level to the F-2s band makes possible a quasiresonant neutralization and therefore, the presence of holes in this AlF_3 band. On the other side, we can infer that the promoted electrons come from the antibonding interaction between the ion and the F-2p band states.

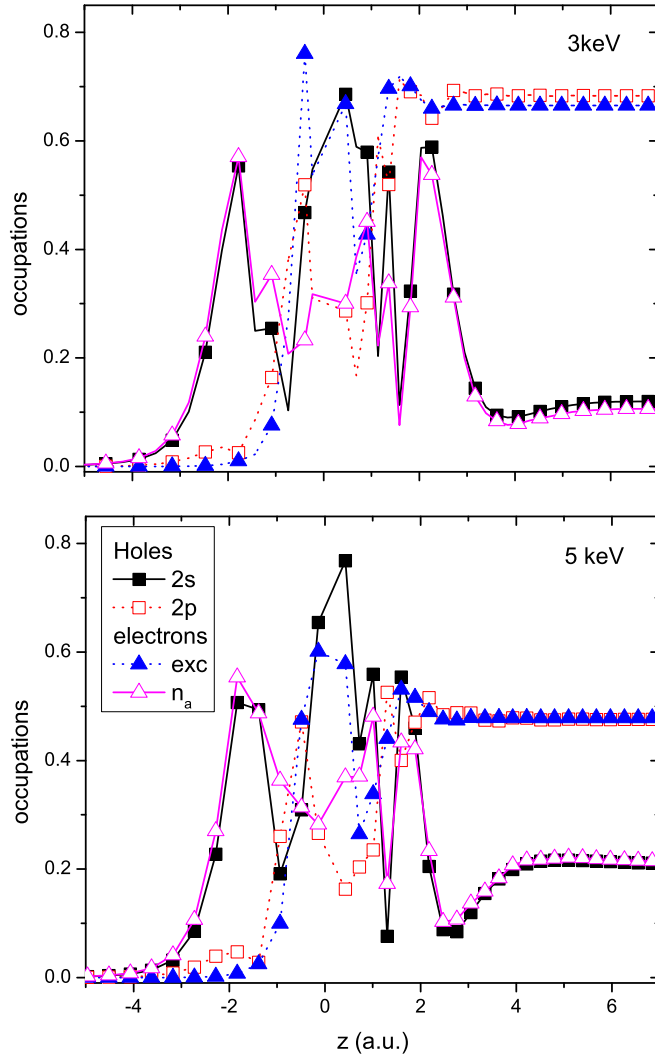


FIG. 7. The hole occupation of F-2s band (full squares), the hole occupation of F-2p band (empty squares), the electron occupation of the projectile state (empty triangles) and the electron occupation of the conduction band (full triangles), as a function of the distance to the surface, z . Incoming ion energy equal to 3 keV in the upper panel and 5 keV in the lower panel.

B. Energy spectra of emitted electrons

The narrow shapes of the electron and hole distributions [Figs. 6(a)–6(c)], strongly governed by the LDOS of AlF_3 surface, imply a large half-life of both, holes, and electrons. It is then justified to calculate the autoionization decay spectra, where the energy of recombination of a hole and an electron is transferred to another electron in the valence band [32] (see Fig. 8). A simple convolution of hole and electron distributions such as the ones shown in Figs. 6(a)–6(c), leads to the emitted electron spectra, $NE(E)$, shown in Fig. 9.

The more energetic emitted electrons with energies between 15 and 25 eV with respect to the vacuum level are originated from the decay of the excited electrons [Fig. 6(c)] to the hole states in the F-2s band (Fig. 6) created due to the He^+ neutralization. Whereas the emitted electrons at energies below 10 eV come from the decay of the excited electrons to the

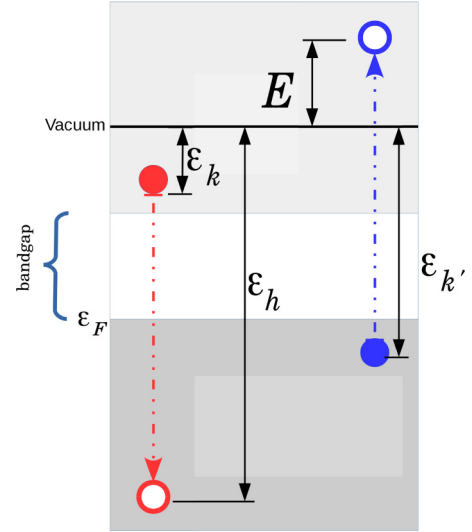


FIG. 8. The autoionization process is shown schematically. An initial excited electron with energy $\varepsilon_{\bar{k}}$ decays to the hole state with energy ε_h ; then, an electron with energy $\varepsilon_{\bar{k}'}$ is emitted to a final state with energy $E = \varepsilon_{\bar{k}} + \varepsilon_{\bar{k}'} - \varepsilon_h$.

hole states in the F-2p band [Fig. 6(b)] originated in the pair electron-hole excitation by the collision process.

The measured energy distributions of emitted electrons do not correspond to the defined ion trajectory in the binary collision process for each incident ion energy (Fig. 9). The experimental spectra are better described if we perform, for each incident kinetic energy, the following weighted sum over different impact parameters, z_{rtp} , taking into account that the weight is proportional to the corresponding area (probability of occurrence):

$$N_T(E) \propto \int dz_{\text{rtp}} z_{\text{rtp}} N E(E, z_{\text{rtp}}). \quad (14)$$

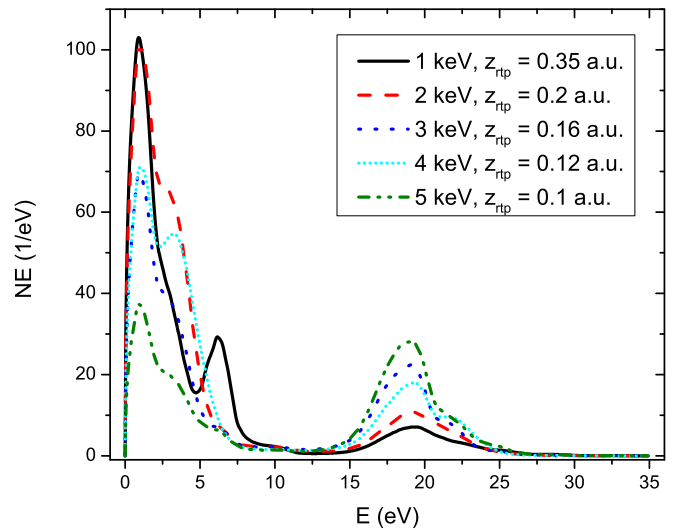


FIG. 9. Energy distribution of emitted electrons for different incoming ion energies. Turning points according to the interaction energy between He^+ and F^\cdot . $E = \varepsilon - W_\phi$.

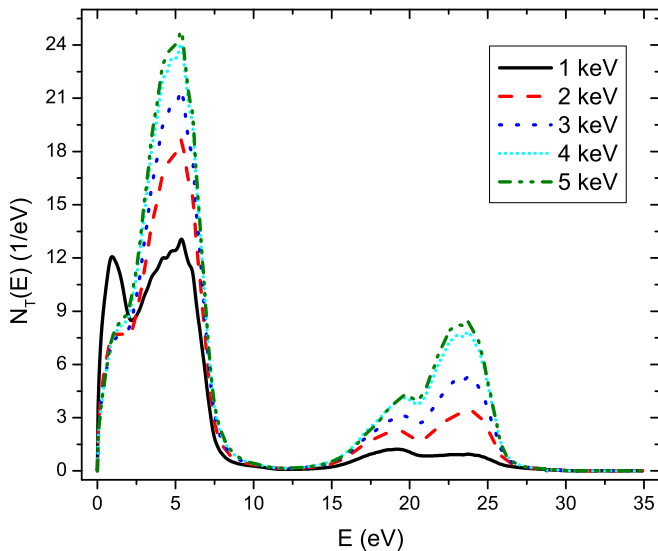


FIG. 10. Energy distribution of emitted electrons for different incoming ion energies. After performing the weighted integration over several impact parameters, Eq. (14). $E = \varepsilon - W_\phi$.

In this form, we obtain the energy spectra of emitted electrons shown in Fig. 10 for different ion kinetic energies. We can observe from Fig. 10 that the high-energy emitted electrons, between 15 and 25 eV, are now reproducing the experimental trends: an increase of the electron emission with the ion kinetic energy.

IV. CONCLUSIONS

We have found that the presence of high-energy electrons in the electron emission from AlF_3 surface when it is bombarded by He^+ , can be explained taking into account the band structure

features of the surface. The strongly localized F-2s band allows for the neutralization of He^+ and therefore, the creation of long-lived holes in this band.

On the other hand, the collision induced excitation of F-2p electrons allows for electrons in the conduction band. The decay of excited electrons to the holes in the F-2s band gives the possibility of having electrons of energies within the observed energy range (10–25 eV).

Then, we can conclude that the ion energy level position relative to the F-2s and F-2p bands is crucial to enable the high-energy electron emission. That is, the proximity of the ion energy level to the F-2s band makes possible a quasideviant neutralization and in this form the presence of holes in this AlF_3 band. On the other side, the promoted electrons come from the antibonding interaction between the ion state and the F-2p band states. We can explain, in this form, the experimental trends of the emitted electron spectra obtained in the case of bombarding with positive ions of Ne and Ar. According to the ionization energy of Ne (21.56 eV), very near to the one for helium, the same mechanism is expected to be operative and efficient. While in the case of Ar, for which the ionization level (15.76 eV) is well above the F-2s band, one expects less contribution from this band to the ion neutralization and therefore, a smaller probability of hole creation. This fact will be evidenced through a diminished intensity of the high-energy secondary electron peak.

ACKNOWLEDGMENTS

This work was supported by CONICET through PIP-112201-50100546CO; UNL through CAI+D grants. C.G. acknowledges financial support from the Spanish Ministry of Economy and Competitiveness, through the “María de Maeztu” Programme for Units of Excellence in R&D (MDM-2014-0377) and the Project MAT2014-59966-R grants.

-
- [1] D. König, R. Scholz, D. R. T. Zahn, and G. Ebest, *J. Appl. Phys.* **97**, 093707 (2005).
- [2] A. Murray, M. Scheinfein, M. Isaacson, and I. Adesida, *J. Vac. Sci. Technol. B* **3**, 367 (1985).
- [3] W. Langheinrich, B. Spangenberg, and H. Beneking, *J. Vac. Sci. Technol. B* **10**, 2868 (1992).
- [4] L. I. Vergara, R. Vidal, and J. Ferrón, *Appl. Surf. Sci.* **229**, 301 (2004).
- [5] G. S. Chen, C. B. Boothroyd, and C. J. Humphreys, *Appl. Phys. Lett.* **69**, 170 (1996).
- [6] E. Kratschmer and M. Isaacson, *J. Vac. Sci. Technol. B* **5**, 369 (1987).
- [7] S. Klein, M. Franco, P. Chardin, and F. Luton, *FEBS Lett.* **579**, 5741 (2005).
- [8] H. Ohno, *Science* **281**, 951 (1998).
- [9] A. H. MacDonald, P. Schiffer, and N. Samarth, *Nat. Mater.* **4**, 195 (2005).
- [10] R. A. Baragiola, *Low-Energy Ion-Surface Interactions* (Wiley, Chichester, England, 1994) Chap. Electron Emission from Slow Ion-Solid Interactions, p. 187.
- [11] *Slow Heavy-Particle Induced Electron Emission from Solid Surfaces*, edited by H. P. Winter and J. Burgdörfer, Springer Tracts of Modern Physics (Springer-Verlag, Berlin, 2007), Vol. 225.
- [12] G. Ruano, R. Vidal, J. Ferrón, and R. Baragiola, *Surf. Sci.* **605**, 1807 (2011).
- [13] H. D. Hagstrum, P. Petrie, and E. E. Chaban, *Phys. Rev. B* **38**, 10264 (1988).
- [14] L. V. Keldysh, *Sov. Phys. JETP* **20**, 1018 (1965).
- [15] L. V. Keldysh, *Zh. Eksp. Teor. Fiz.* **47**, 1515 (1964).
- [16] P. Daniel, A. Bulou, M. Rousseau, J. Nouet, J. L. Fourquet, M. Leblanc, and R. Burriel, *J. Phys.: Condens. Matter* **2**, 5663 (1990).
- [17] J. O. Lugo, E. C. Goldberg, E. A. Sánchez, and O. Grizzi, *Phys. Rev. B* **72**, 035432 (2005).
- [18] J. O. Lugo, E. C. Goldberg, E. A. Sánchez, and O. Grizzi, *Phys. Rev. B* **72**, 035433 (2005).
- [19] A. Kokalj, *Comput. Mater. Sci.* **28**, 155 (2003).
- [20] J. P. Lewis, K. R. Glaesemann, G. A. Voth, J. Fritsch, A. A. Demkok, J. Ortega, and O. F. Sankey, *Phys. Rev. B* **64**, 195103 (2001).
- [21] P. Jelinek, H. Wang, J. P. Lewis, O. F. Sankey, and J. Ortega, *Phys. Rev. B* **71**, 235101 (2005).

- [22] D. D. Felice, E. Abad, C. González, A. Smogunov, and Y. J. Dappe, *J. Phys. D: Appl. Phys.* **50**, 17LT02 (2017).
- [23] H. D. Hagstrum, *Phys. Rev.* **96**, 336 (1954).
- [24] A. Iglesias-García, E. A. García, and E. C. Goldberg, *Phys. Rev. B* **90**, 195416 (2014).
- [25] A. Iglesias-García, E. A. García, and E. C. Goldberg, *Phys. Rev. B* **87**, 075434 (2013).
- [26] P. G. Bolcatto, E. C. Goldberg, and M. C. G. Passeggi, *Phys. Rev. B* **58**, 5007 (1998).
- [27] F. J. Bonetto, M. A. Romero, A. Iglesias-García, R. A. Vidal, and E. C. Goldberg, *J. Phys. Chem. C* **119**, 3124 (2015).
- [28] P. O. Lowdin, *J. Chem. Phys.* **18**, 365 (1950).
- [29] S. Huzinaga, J. Andzelm, M. Klobukowsky, E. Radzio-Andzelm, Y. Sakai, and H. Tatewaki, in *Gaussian Basis Set for Molecular Calculation*, edited by S. Huzinaga (Elsevier, Amsterdam, 1984).
- [30] S. Huzinaga, *J. Chem. Phys.* **42**, 1293 (1965).
- [31] C. Cohen-Tannoudji, B. Diu, and F. Laloe, *Quantum Mechanics* (Wiley, New York, 1991), Vol. 1.
- [32] N. Bajales, L. Cristina, S. Mendoza, R. A. Baragiola, E. Goldberg, and J. Ferrón, *Phys. Rev. Lett.* **100**, 227604 (2008).